

Remodeling of Fracture Callus in Mice Is Consistent with Mechanical Loading and Bone Remodeling Theory

Hanna Isaksson,^{1,2} Ina Gröngröft,¹ Wouter Wilson,² Corrinus C. van Donkelaar,² Bert van Rietbergen,² Andrea Tami,¹ Rik Huiskes,² Keita Ito^{1,2}

¹AO Research Institute, Davos, Switzerland, ²Department of Biomedical Engineering, Eindhoven University of Technology, Postbox 513, WH3.116, 5600 MB Eindhoven, The Netherlands

Received 30 October 2007; accepted 12 May 2008

Published online 4 November 2008 in Wiley InterScience (www.interscience.wiley.com). DOI 10.1002/jor.20725

ABSTRACT: During the remodeling phase of fracture healing in mice, the callus gradually transforms into a double cortex, which thereafter merges into one cortex. In large animals, a double cortex normally does not form. We investigated whether these patterns of remodeling of the fracture callus in mice can be explained by mechanical loading. Morphologies of fractures after 21, 28, and 42 days of healing were determined from an in vivo mid-diaphyseal femoral osteotomy healing experiment in mice. Bone density distributions from microCT at 21 days were converted into adaptive finite element models. To assess the effect of loading mode on bone remodeling, a well-established remodeling algorithm was used to examine the effect of axial force or bending moment on bone structure. All simulations predicted that under axial loading, the callus remodeled to form a single cortex. When a bending moment was applied, dual concentric cortices developed in all simulations, corresponding well to the progression of remodeling observed experimentally and resulting in quantitatively comparable callus areas of woven and lamellar bone. Effects of biological differences between species or other reasons cannot be excluded, but this study demonstrates how a difference in loading mode could explain the differences between the remodeling phase in small rodents and larger mammals. © 2008 Orthopaedic Research Society. Published by Wiley Periodicals, Inc. *J Orthop Res* 27:664–672, 2009

Keywords: fracture healing; bone remodeling; mechanobiology; mouse femur; finite element analysis

Bone fracture repair is a complex process divided into inflammatory, soft and hard callus reparative, and remodeling phases.^{1,2} Most current research focuses on the reparative phase, during which bone stiffness is restored.^{3,4} Hardly any studies have characterized the remodeling phase, although in this phase full strength returns and the chance of refracture decreases.⁵

Remodeling is replacement of woven bone, rapidly laid down in the reparative phase, by lamellar bone.⁴ Callus is slowly resorbed until the original bone shape is restored.^{6,7} Endosteal callus resorption also coincides with reestablishment of the intramedullary canal and the original blood supply.⁸ Fluid shear stresses in bone are thought to modulate these activities.⁹

Animal models, particularly mice, are frequently used to study fracture repair.^{10–15} The availability of knockout mice and the elucidation of the murine genome have extended the importance of murine models.^{2,16,17} Inflammatory and reparative phases of fracture healing are similar to those in larger mammals. However, the remodeling phase has not been thoroughly investigated.

During analysis of a murine model of fracture repair, a phenomenon was noted that differs from that in large mammals.^{18,19} At the end of the reparative phase, an external large callus had developed, similar to that in large animals, and periosteal and endosteal bony bridging was achieved. However, during remodeling, the callus gradually transformed into double, concentric cortices. Later, the two cortices, equally thick and dense, merged through remodeling. This behavior has not been described in literature, but seems to occur in fracture remodeling in rodents undergoing secondary healing

with relative stability.²⁰ Why do mice respond differently than larger mammals during bone fracture remodeling? The difference might be due to biological differences between species or to distinct mechanical loading patterns. It is important to identify if it is the former, since often results in mice are related to what would be expected in humans.

This study describes the remodeling phase in mice and aims to provide a plausible explanation for the differences between rodents and larger mammals.^{18,19} During murine gait, the knee and ankle are always flexed, whereas in human gait, the knee and ankle are more extended. We hypothesized that differences in bone geometry during the remodeling phase of fracture healing in mice compared to larger mammals is due to differences in mechanical loading. An established bone remodeling theory was used,^{21,22} in which adaptation of bone mass and geometry over time were modulated through osteocyte mechano-sensing and signaling. The predicted bone distributions for various loading cases were then compared to the remodeling behavior observed in an in vivo murine fracture healing model.

MATERIALS AND METHODS

Fracture Healing Model

The in vivo experiment was part of a larger study, characterizing fracture healing with rigid and flexible plate fixation.^{18,19} Part of that experiment (late time points with flexible plates) was reanalyzed and used to determine fracture healing callus morphology during the remodeling phase. Briefly, a flexible plate was attached to the anterior aspect of the mid-femur through a lateral approach²³ (Fig. 1a) to stabilize a 0.45-mm mid-diaphyseal gap osteotomy in female C57BL/6 mice, 20–25 weeks old (Fig. 1b). All procedures were approved by the Animal Experimentation Commission of the Veterinary Office of the Canton of Grisons.

Mice were able to freely weight-bear postoperatively. They were euthanized after 21, 28, or 42 days of healing ($n = 10$ per

Correspondence to: Keita Ito (T: +31 40 247 3851; F: +31 40 247 3744; E-mail: k.ito@tue.nl)

© 2008 Orthopaedic Research Society. Published by Wiley Periodicals, Inc.

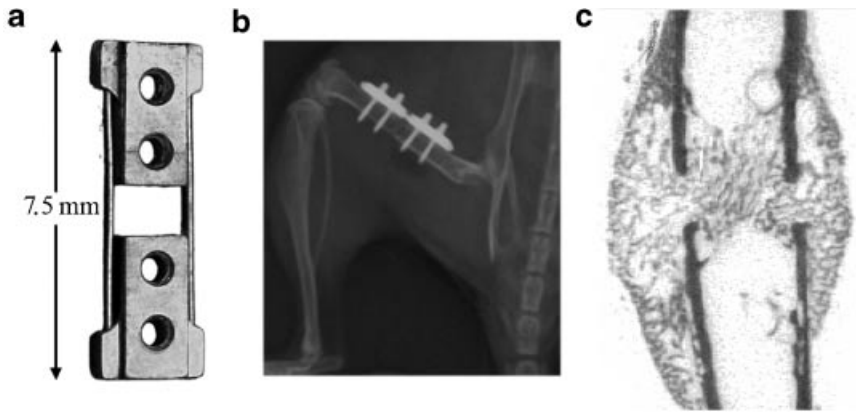


Figure 1. (a) Flexible locked bridging pate used in the experimental study^{18,19,23}; (b) postoperative radiograph; (c) FE mesh created from a mid-sagittal section of the microCT reconstruction after 21 days healing. This was assumed to be the starting point for remodeling.

healing duration). After excision, four-point bending stiffness of the osteotomized femur was determined as a percentage of the stiffness of the contralateral femur by nondestructive mechanical testing. The femora were then fixed in methanol for 10 days. Thereafter, μ CT imaging of the healing bones was performed (μ CT 40, Scanco Medical, Bassersdorf, Switzerland), with an isotropic voxel resolution of 12 μ m. Three-dimensional segmented reconstructions were used for qualitative evaluation of sub-volumes of the bone. A thresholding algorithm protocol was used to segment tissue into three attenuation types, i.e., soft tissue (<145), newly formed woven bone (low mineralization, 145–360), and lamellar bone (high mineralization, >360, in per mille of maximal image gray values).²⁴

For histological analysis, femora of eight mice per time point were embedded in methylmethacrylate, and serially sectioned on a circular saw. The mid-longitudinal section of each femur was stained with 1% Toluidine blue (Fluka) for 15 min and blot dried after washing in deionized water. Sections in the region between the outer screw holes were examined with a macrofluoroscope at $\times 64$ magnification (MacroFluo,TM Leica Microsystems, Heerbrugg, Switzerland). A custom macro (AxioVision, KS400, Zeiss) was used to measure the area of woven bone, lamellar bone, cartilage, and total callus.

Bone Remodeling

Bone remodeling was simulated based on a well-established theory.^{21,22} It assumes that osteocytes sense local strain-energy-density (SED) and send a corresponding signal to the bone surface, which either activates osteoblasts or inhibits osteoclasts. The signals are assumed to decay exponentially with distance, so only osteocytes within a distance ($d(x, x_k)$) smaller than the decay distance D are included when calculating the total stimulus P , given by the sum of all signals within the influence distance of location x :

$$P(x, t) = \sum_{k=1}^n \left(\exp\left(\frac{-d(x, x_k)}{D}\right) \cdot \mu U_k \right) \quad (1)$$

where n = the number of osteocytes within the influence volume, μ = the osteocyte mechanosensitivity, and U_k = the SED-rate sensed by osteocyte k . Bone is resorbed when $P <$ the resorption threshold C_{tr} , or by random microcracks formed in the bone.²¹ The resorption probability is:

$$p_{resorb} = R_{max} - \frac{R_{max}}{C_{tr}} P(x, t), \quad (2)$$

where R_{max} is the maximal chance of resorption. Osteoclasts are assumed to resorb a fixed amount of bone, so the change in

bone volume due to resorption at any time point (dV_r/dt) is:

$$\frac{dV_r(x, t)}{dt} = V_{cl}, \quad (3)$$

where V_{cl} is the amount of bone resorbed by one osteoclast. When the local stimulus $>$ the formation threshold k_{tr} , bone formation will occur. The amount of bone formed (dV_f/dt) is:

$$\frac{dV_f(x, t)}{dt} = \tau(P(x, t) - k_{tr}), \quad (4)$$

where τ is a material constant (the proportionality factor). The change in bone volume is the sum of the resorbed and deposited bone volumes; the total amount of bone in each integration point is then updated. Based on the local amount of bone, local bone volume density ρ is calculated, which allows the homogenized stiffness of the volume to be updated:

$$E = E_{max} \rho(x, t)^\gamma, \quad (5)$$

where E_{max} is the maximal bone stiffness and γ a material constant.^{25,26} The remodeling theory was implemented into ABAQUS v. 6.5 (Simulia, Dassault Systemés). The osteocytes were positioned at random locations. The reference volume was chosen as $1/4$ of the elemental volume (integration-point volume). The number of osteocytes per integration point volume V_{ip} was:

$$n_{osteo} = V_{ip} \rho_{osteo}, \quad (6)$$

where ρ_{osteo} is the osteocyte density. When more bone was to be formed than the free volume available within the integration point volume, the rest of the bone volume formed was distributed over the surrounding integration point volumes. The same was done for over resorption, when more bone was resorbed than what was present. All the parameters employed by the remodeling theory are given in Table 1.

Micro-CT Imaging and Conversion

Fracture calluses after 21 days of healing were assumed to be starting points for the remodeling phase. Eight of nine calluses showed comparable morphology; five representative bones were chosen for the simulations. Using the μ CT images, bone tissue was segmented from soft tissue, and the full range of output bone density data was converted to mineral content and bone density. Two-dimensional mid-sagittal sections were converted to 2D finite element meshes, where each voxel provided initial bone density for one integration point (Fig. 1c). Each linear four-node plain strain element was $24 \times 24 \mu$ m. Bone was modeled as a homogenous linear isotropic material with a Poisson's ratio of 0.3 and a maximum Young's modulus

Table 1. Parameters and Constants Used for the Bone Remodeling Theory

Variable	Symbol	Unit	Value
Osteocyte density	n	mm^{-3}	$96,000^{50}$
Osteocyte mechanosensitivity	μ	$\text{mol mm J}^{-1} \text{s}^{-1} \text{day}^{-1}$	1.0
Osteocyte influence distance	D	μm	50^{51}
Formation threshold	k_{tr}	$\text{mol mm}^{-2} \text{day}^{-1}$	2.0×10^{-4}
Proportionality factor	τ	$\text{mm}^5 \text{mol}^{-1}$	5.0×10^{-4}
Resorption amount per cavity	R	mm^3	$1.5 \times 10^{-3} \text{ }^{52}$
Maximum elastic modulus bone	E_{max}	GPa	5.0^{27}
Poisons ratio	ν		0.3
Exponent gamma	γ		$3.0^{25,26}$

of 5 GPa.²⁷ Elements with no bone were assumed to be marrow and were modeled with the same Poisson's ratio but with a Young's modulus of 1 MPa. Areas were classified as woven or lamellar, according to the same thresholds as employed experimentally, and were used to quantitatively compare experimental and computational results.

Determination of Loading Conditions

In large mammals, loading is well defined both in direction and magnitude, whereas in mice the loading is mostly unknown. To investigate if direction of loading could explain bone remodeling differences observed between mice and larger mammals, we assumed two loading modes, an axial force or a bending

moment. The force was tied to all nodes on the proximal cortical ends, while the distal ends were rigidly fixed, and was applied either in the y-direction (axial) or around the z-axis, resulting in a bending moment (Fig. 2a). The load magnitudes in mice are unknown, so they were estimated by running the remodeling simulation with various loads on an unfractured cortex, applied both axially and as a moment. The magnitudes were from 0.20 N, 0.5 N, 0.75 N, 1 N, 2N, 3 N, and 5 N. The magnitudes that resulted in steady-state cortical geometry similar to intact femora were selected (Fig. 2b), and used for simulations of the experimentally collected 21 day calluses. Predictions from day 21 onward were compared with the experimental results after 28 and 42 days.

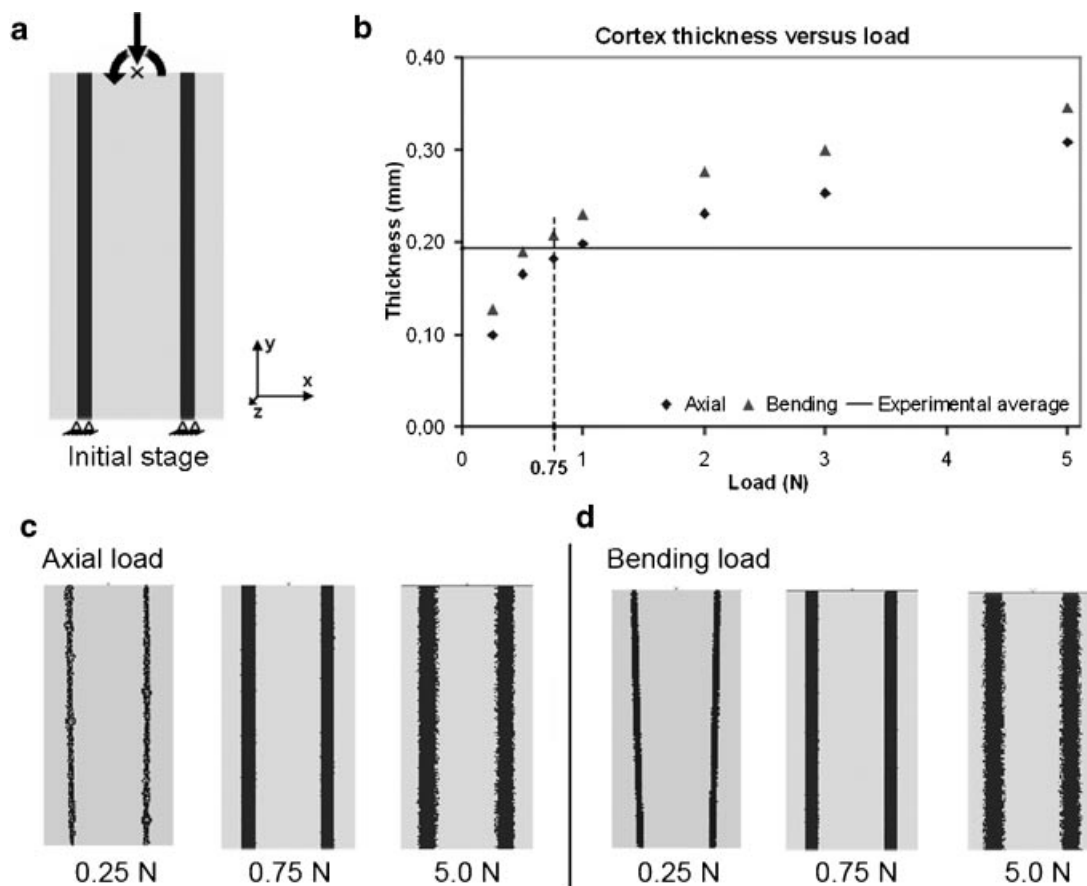


Figure 2. (a) A force was applied with varying magnitudes axially (y) or around the bending axis (z); (b) 0.75 N was chosen since it resulted in steady state cortical thicknesses that were close to those measured experimentally. The resulting moment at the fracture site was 1.8 Nmm; (c, d) steady state diameters recorded (c) axially and (d) under bending with loads of 0.25 N, 0.75 N, and 5.0 N.

Table 2. Experimental Data Are Mean (\pm SD) Values from All Analyzed Mice

	21 Days	28 Days	42 Days
Mechanical testing			
Stiffness %	50% (\pm 15%)	61% (\pm 16%)	74% (\pm 20%)
MicroCT (mm^3)			
Woven bone	4.5 (\pm 0.7)	2.7 (\pm 0.8)	1.0 (\pm 0.3)
Lamellar bone	2.6 (\pm 0.4)	3.3 (\pm 0.5)	3.1 (\pm 0.3)
MicroCT dual cortex (DC)			
DC/total mice	0/9	6/9	6/6
Histomorphometry (mm^2)			
Woven bone	1.8 (\pm 0.4)	0.5 (\pm 0.3)	0.4 (\pm 0.2)
Lamellar bone	0.3 (\pm 0.1)	1.6 (\pm 0.5)	1.7 (\pm 0.4)
Cartilage	0.06 (\pm 0.09)	0.08 (\pm 0.2)	0.06 (\pm 0.1)

RESULTS

Experimental Callus Remodeling

One of 10 animals in the 21- and 28-day groups and 4 of 10 in the 42-day group were excluded due to malunion or technical problems during plate removal. At 21 days, radiographs exhibited abundant callus; callus size peaked around 21 days then decreased to day 42. Between 21 and 42 days, the stiffnesses of the femora increased from 50% to 74% of that in the contralateral intact femora (Table 2).¹⁸ Quantitative microCT showed that the amount of newly formed woven bone was greater at day 21 compared to later time points, while the amount of lamellar bone was greater at days 28 and 42 (Table 2). Callus remodeling began around day 21, when woven bone was evenly distributed in the callus (Fig. 3a, b). After 28 days, most the woven bone within the periosteal callus was resorbed, while the periosteal part of the callus and the direct cortical gap continued to densify (Fig. 3c, d). A dual cortex developed in six of nine mice and was under development in the remaining

three. Some endosteal callus remained, with mainly new woven bone in the gap and in the outer cortex. By 42 days, most endosteal callus had resorbed. The double cortices, visible in all mice, were equally thick and the bone directly bridging the gap and the bone in the outer double cortex was mostly highly mineralized lamellar bone. The callus diameters and the distances between the cortices were smaller at 42 days than at 28. Histomorphometry confirmed that the amount of woven bone decreased between day 21 and day 42, while the amount of lamellar bone increased (Table 2). The double cortex formation was also visible histologically (Fig. 4). It developed between 21 and 28 days and was smaller but still present at 42 days.

Computational Predictions

Figure 2c, d shows variations in steady state geometries with some of the load magnitudes that were investigated. A force of 0.75 N was chosen and applied either axially or around the bending axis (Fig. 2b). Under axial

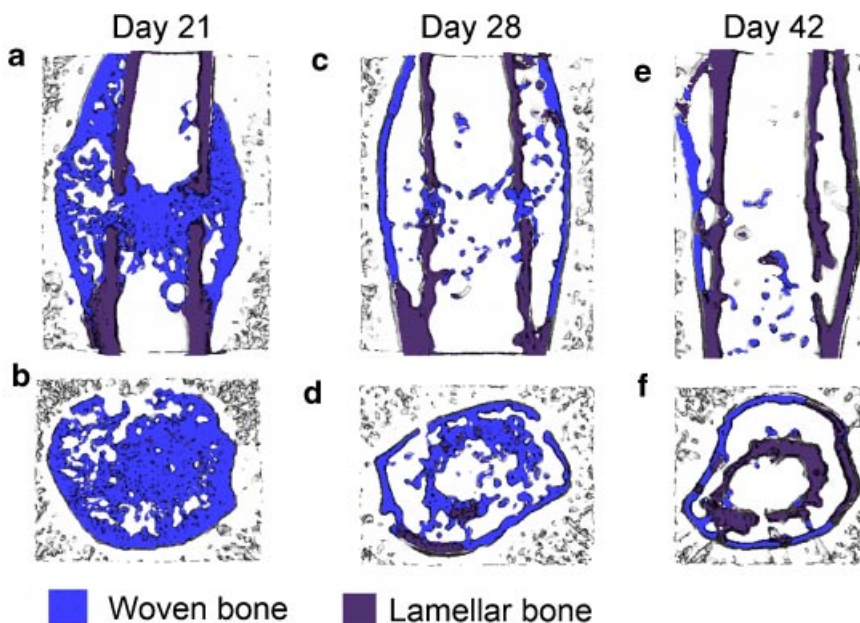


Figure 3. Examples of microCT data at (a, b) 21, (c, d) 28, and (e, f) 42 days. (a), (c), and (e) show mid-sagittal sections; and (b), (d), and (f) transverse sections through the fracture gap.

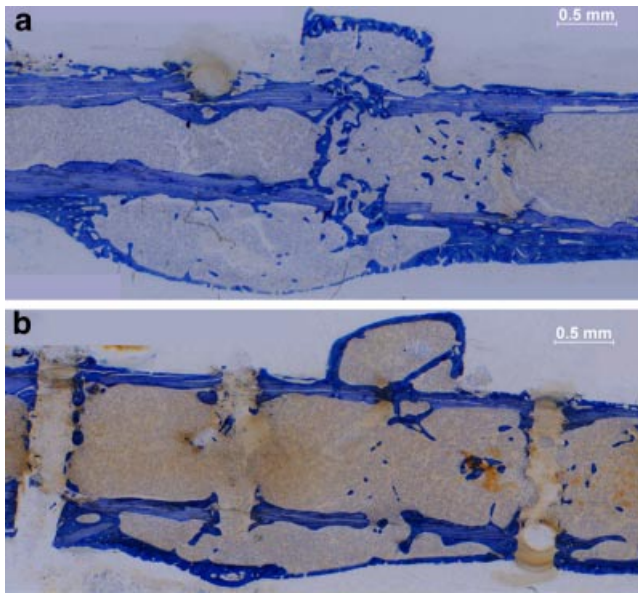


Figure 4. Mid-sagittal histology through the gap after (a) 28 days and (b) 42 days (Toluidine blue, plate position, above). The upper periosteal area is partly blocked by the plate, and bridging in the external callus was only possible in the area of the wires. Double cortex formation is visible at 28 days; at 42 days, the callus size was reduced as woven bone was remodeled into lamellar bone.

load similar evolution of bone distributions was predicted in all five samples. Remodeling was relatively fast with subsequent resorption of the periosteal callus (Fig. 5a). The density close to the cortex and surrounding the fracture gap increased. Thereafter, most of the endosteal callus was resorbed with a further density increase in the gap. By iteration 30, little endosteal callus remained. After 50 iterations, the cortex was nearly restored, and after 100 iterations, no evidence of the fracture existed (Fig. 5a).

Under bending load, similar evolution of bone distributions was predicted in all five samples. However, the spatial and temporal distributions differed significantly from those predicted under axial load (Fig. 5b). Initially, the external periosteal-callus shell and the cortical gap became gradually denser, while trabecular bone inside the periosteal callus was resorbed. Thereafter, resorption of the endosteal callus initiated, while the gap and periosteal shell became even denser. After iteration 25, a dual cortex had developed. Most of the newly developed cortex had a lower bone density than the original cortex, but over time, both cortices were of equally high density. After iteration 50, the dual cortex slowly remodeled through periosteal resorption and endosteal apposition, and the original cortex was restored (iteration 150).

Comparison between Experimental and Simulated Results

There was no resemblance between experimental data at 28 and 42 days and the axial load simulations. Computationally, the entire callus was resorbed and the original cortex restored, as evidenced from the SED distributions (Fig. 6). The SED between days 21 and 28 showed high stimulation at the cortex and the fracture gap, comparing well with normal healing in larger mammals. In contrast, simulations loading the callus in bending corresponded well with bone remodeling observed in mice with a dual cortex that became denser and thicker and then merged. Experimentally the merging of the dual cortex was not observed, but the distance between cortices at day 42 was less than after 28 days, indicating that they were merging. The SED distributions after iteration 5 of the bending simulations (Fig. 6) showed the same progression, where both periosteal callus line and the gap formed bone. The SED distributions clearly showed differences between

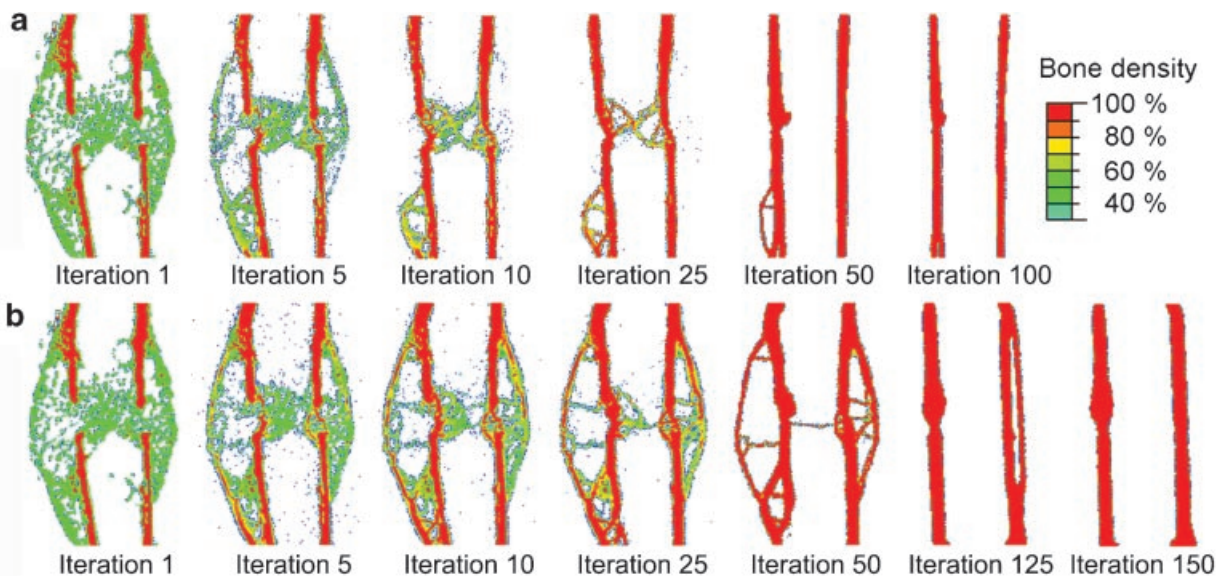


Figure 5. Predicted bone distributions and densities during callus remodeling starting from 21 days. (a) With axial load, periosteal callus gradually resorbed, followed by endosteal callus. Lamellar bone bridged the fracture gap between iterations 10–25; at 100, the original cortex was restored. (b) With bending, a dual cortex developed; the external periosteal callus and the gap remodeled into high density lamellar bone (iteration 25). Thereafter, the dual cortex merged together slowly, and one single cortex was restored after 150 iterations.

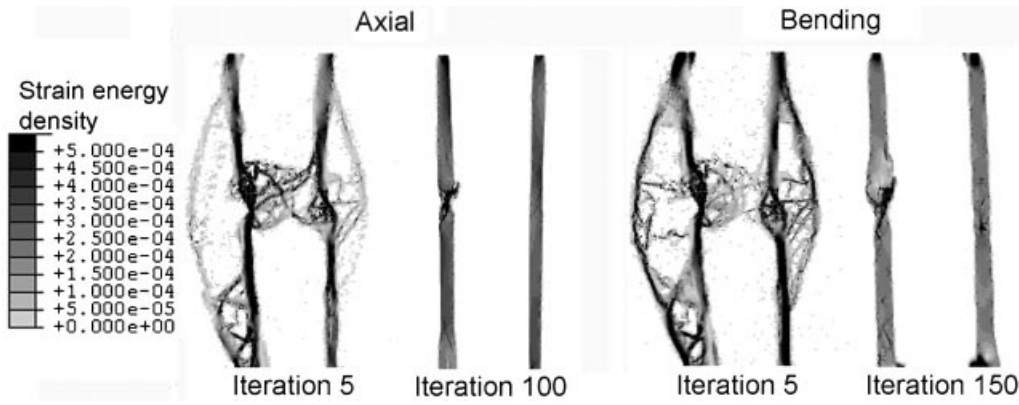


Figure 6. SED distributions explain observed differences in remodeling. Dark gray displays where bone will form; light gray where resorption occurs. With axial load (left), after 5 iterations, SED is stimulating formation primarily in the gap, and external callus resorbs rapidly. With bending (right), the external callus and the cortical gap experience high SED.

mechanical stimulation axially and under bending. During the first couple of iterations, the dark areas of SED predicted a double cortex from bending, while load transmission from axial stimulation predicted that the callus would be resorbed. After 100 (axial) or 150 (bending) iterations, a small “bony bump” remained on the cortex at the former location of the fracture gap. The SED distributions indicated that this area would be restored over time.

Quantitative comparison indicated that the total callus area and areas of newly formed woven and lamellar bone calculated by the computational model in bending were similar to those determined histomorphometrically (Fig. 7). However, the time sequence was slower. Still, all computationally quantified areas (except the woven bone area at 28 days) were within a standard deviation of the experimental results.

DISCUSSION

The mechanical loading mode could explain the remodeling characteristics of fracture healing in small rodents compared to larger mammals, including temporary dual cortex formation during postfracture remodeling in mice. The progression of healing and remodeling in mice was monitored experimentally and compared

qualitatively and quantitatively to simulations with bone remodeling theory under different loading modes. Simulations on data from five animals were the same. The simulated callus patterns for loading in bending matched the experimentally remodeled bone morphologies in mice after 28 and 42 days. With axial load, no similarities were found between predictions and actual mice fracture healing patterns. Instead, bone density distributions resembled remodeling during fracture healing in larger mammals. Hence, murine remodeling could be explained by a difference in mechanical loading mode, which may result from their skeletal structure or posture differences during gait.

The experimental model demonstrated formation of a double cortex during remodeling phase of healing. It developed around 28 days post fracture (6/9 mice) and was evident in all animals after 42 days of healing. Most investigators focused on other aspects of healing^{12,13,28,29} or ended their experiments prior to remodeling.^{28,30,31} However, three studies included radiographs after 4 weeks of healing in a rat femur in which a double cortex can be recognized.^{29,32,33} Gerstenfeld et al.³⁴ provided a 3D microCT reconstruction of fracture callus morphogenesis. This study shows signs of double cortex formation in a rat femur after 35 days of healing. Hence, this appears to be a general phenomenon in rodents undergoing secondary fracture healing. Since mouse models are used in studies of bone healing, the biological behavior in mice should be comparable to that in humans if the desire is to extrapolate the results to physiological and clinical problems encountered in humans. Our study provides a mechanical explanation for differences in the remodeling phase, so the formation of a dual cortex does not have to be seen as a biological difference between species.

The loading carried by the femoral diaphysis is determined by joint reactive forces, joint positions and muscular forces which are unknown in mice. Therefore, we employed two extremes, axial and bending loads. All additional muscle forces were neglected. The loading conditions in humans^{35,36} and larger mammals such as sheep^{37,38} are well described. Large quadrupeds are commonly used for fracture studies because of their similarity in long bone loading to humans. All long bones

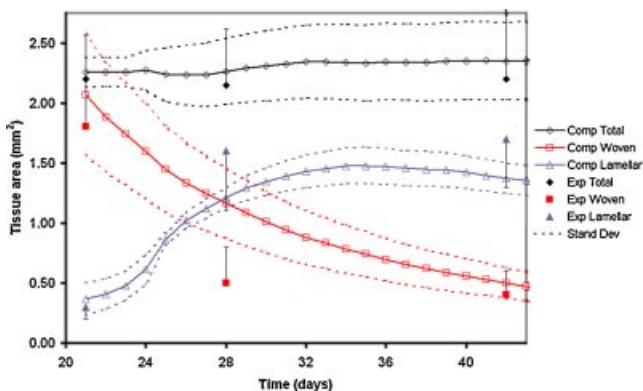


Figure 7. Comparison of computationally calculated tissue areas and equivalent experimentally measured data at 21, 28, and 42 days postfracture (mean ± SD). Dotted lines display standard deviations from the computational analysis.

experience significant bending moments, likely to give them their tubular shape. However, the amount of bending moments in these mammals relative to the amount of axial load is low. Unfortunately, for rats and mice only ground reaction forces are available.^{39,40} It can be argued that the differences in joint position in mice most likely result in a difference in mechanical loading on the bone. However, to our knowledge there is yet no evidence of this. In human gait, the effect of flexed hip and knee positions can be seen by comparing stair climbing with mid-stance walking. The maximum load is not too different, but differences exist in the relative medial–lateral, anterior–posterior and proximal–distal components.³⁶ Stair climbing results in larger relative bending moments than walking, so animals with flexed joints might also have higher amounts of bending moments in their femora. One study characterized knee biomechanics in rabbits,⁴¹ providing insight in the differences in relative forces and moments compared to larger animals. From that study it can be anticipated that there would be larger bending moments on the femora in small animals such as mice. Finally, studies that have characterized mouse gait are consistent, and reported ground reaction forces corresponding with those we used.

The proximal and distal ends of the cortex in the computational model were tied to ensure that their relative distance remained constant, and that the full 3D structure of the cortex was mimicked. No out-of-plane loads were applied. The resulting bone morphology was therefore only analyzed in the loading plane. Experimentally, double cortices were formed around the entire femora (Fig. 3e), except at the plate attachment site. For this phenomenon to be captured by the model in 3D, bending moments in all directions are necessary. A 2D model was chosen because a 3D model would be computationally expensive and would require better characterized loading conditions. Our 2D model is therefore only valid in the plane of bending. Nevertheless, a 2D geometry and simplified loading as used in this study can serve to provide a possible explanation for why remodeling behavior is different in mice compared to larger mammals. In addition, the bone remodeling theory does not account for contributions from cartilage completely. However, the cartilage remaining after 21 days was small (Table 2), so its contribution to the callus stiffness was assumed low. Moreover, the flexible plate was not included in the model. This likely had only minor influences, since the loads were modulated with the remodeling algorithm to find the magnitudes that resulted in normal cortex diameters, and the microCT data from medial–lateral plane was used, while the plate was applied on the anterior aspect of the femur.

The parameter values were adopted from Ruimerman et al.,²² except for when direct data from murine studies could be found (Table 1). The model assumes a constant osteocyte density over different bone types and densities and over time. However, areas of high bone turnover, such as fracture callus, are characterized by a high

number of cells.⁴² The osteocyte populations in woven bone are believed to be larger than in lamellar bone^{43,44} and to decrease with remodeling until normal levels are restored. A recent study concluded that densities in the central callus region are about 100% larger than in normal lamellar bone⁴⁵ and that osteocyte density in woven bone formed during healing through intramembranous or endochondral pathways can be different.⁴⁵ We could implement this by starting the stimulation with variations in osteocyte densities depending on initial bone density, and then updating those during remodeling. However, Mullender et al.⁴⁶ showed that osteocyte density in the model only affected remodeling rate, not the remodeling pattern. Hence, it would not affect the conclusion of our study.

Computational models of fracture repair have previously focused on the reparative phase.^{47,48} Some models have included simplified conditions for remodeling or resorption of the callus.^{47,48} The complexity shown in murine fracture healing during the remodeling phase, including the double cortex formation, suggests that a more detailed model such as a bio-physical bone remodeling theory should be used. The fact that these contrasting differences in postfracture remodeling between species was induced by different loading patterns supports the hypotheses underlying load-based bone remodeling theories.²¹

The remodeling algorithm applies to cortical and trabecular bone remodeling²² and describes osteoporotic changes.⁴⁹ However, it has not previously been used or validated on whole bones or in fracture repair. In this study, the unifying theory was applied to small animals for the first time. Although mice bones are different in many aspects, the study was successful. Equally as important, the study also showed that the theory²¹ applies to remodeling during regeneration.

In conclusion, the bone remodelling theory predicts the distinct remodeling patterns seen in mice, including dual cortex formation when a bending load is applied. Despite that other reasons for the observed differences between mice and humans cannot be excluded, this study has shown that it could be explained by differences in mechanical loading. Hence, it does not necessarily arise from biological differences.

ACKNOWLEDGMENTS

The authors acknowledge financial support from the AO Foundation, Switzerland.

REFERENCES

1. Cruess RL, Dumont J. 1975. Fracture healing. *Can J Surg* 18:403–413.
2. Einhorn TA. 1998. The cell and molecular biology of fracture healing. *Clin Ortho* p S7–S21.
3. Einhorn TA. 1995. Enhancement of fracture-healing. *J. Bone Joint Surg [Am]* 77:940–956.
4. Marsh DR, Li G. 1999. The biology of fracture healing: optimising outcome. *Br Med Bull* 55:856–869.
5. Ruedi TP, Buckley RE, Moran CG. 2007. *AO principles of fracture management*. 2nd ed. Davos, Switzerland: AO Publishing.

6. Owen M. 1970. The origin of bone cells. *Int Rev Cytol* 28:213–238.
7. Willenegger H, Perren SM, Schenk R. 1971. [Primary and secondary healing of bone fractures]. *Chirurg* 42:241–252.
8. Rhinelander FW. 1968. The normal microcirculation of diaphyseal cortex and its response to fracture. *J Bone Joint Surg [Am]* 50:784–800.
9. Bakker A, Klein-Nulend J, Burger E. 2004. Shear stress inhibits while disuse promotes osteocyte apoptosis. *Biochem Biophys Res Commun* 320:1163–1168.
10. Cheung KM, Kaluarachi K, Andrew G, et al. 2003. An externally fixed femoral fracture model for mice. *J Orthop Res* 21:685–690.
11. Hiltunen A, Vuorio E, Aro HT. 1993. A standardized experimental fracture in the mouse tibia. *J Orthop Res* 11:305–312.
12. Holstein JH, Menger MD, Culemann U, et al. 2007. Development of a locking femur nail for mice. *J Biomech* 40:215–219.
13. Manigrasso MB, O'Connor JP. 2004. Characterization of a closed femur fracture model in mice. *J Orthop Trauma* 18:687–695.
14. Thompson Z, Miclau T, Hu D, et al. 2002. A model for intramembranous ossification during fracture healing. *J Orthop Res* 20:1091–1098.
15. Tay BK, Le AX, Gould SE, et al. 1998. Histochemical and molecular analyses of distraction osteogenesis in a mouse model. *J Orthop Res* 16:636–642.
16. Mundlos S, Olsen BR. 1997. Heritable diseases of the skeleton. Part I: molecular insights into skeletal development-transcription factors and signaling pathways. *FASEB J* 11:125–132.
17. Mundlos S, Olsen BR. 1997. Heritable diseases of the skeleton. Part II: molecular insights into skeletal development-matrix components and their homeostasis. *FASEB J* 11:227–233.
18. Gröngröft I, Heil P, Matthys-Mark R, et al. 2007. Fixation compliance in a murine fracture model induces two different processes of fracture healing but does not lead to delayed union. 6th Combined Meeting of the ORS, Honolulu, Hawaii, October 20–24, 2007.
19. Heil P, Gröngröft I, Matthys-Mark R, et al. 2006. Flexible fixation-induced delayed fracture healing in a murine fracture model [5th World Congress of Biomechanics, abstract]. *J Biomech* 39:S467.
20. Gerstenfeld LC, Alkhiary YM, Krall EA, et al. 2006. Three-dimensional reconstruction of fracture callus morphogenesis. *J Histochem Cytochem* 54:1215–1228.
21. Huiskes R, Ruimerman R, van Lenthe GH, et al. 2000. Effects of mechanical forces on maintenance and adaptation of form in trabecular bone. *Nature* 405:704–706.
22. Ruimerman R, Hilbers P, van Rietbergen B, et al. 2005. A theoretical framework for strain-related trabecular bone maintenance and adaptation. *J Biomech* 38:931–941.
23. Matthys-Mark R, Perren SM. 2008. Internal fixation systems for improved genetic and biomechanical studies in mice. Transactions of the 54th ORS 2008, San Francisco, CA; abstract 1005.
24. Gabet Y, Muller R, Regev E, et al. 2004. Osteogenic growth peptide modulates fracture callus structural and mechanical properties. *Bone* 35:65–73.
25. Carter DR, Hayes WC. 1977. The compressive behavior of bone as a two-phase porous structure. *J Bone Joint Surg [Am]* 59:954–962.
26. Currey JD. 1988. The effect of porosity and mineral content on the Young's modulus of elasticity of compact bone. *J Biomech* 21:131–139.
27. Schriefer JL, Robling AG, Warden SJ, et al. 2005. A comparison of mechanical properties derived from multiple skeletal sites in mice. *J Biomech* 38:467–475.
28. Meyer MH, Meyer RA Jr. 2007. Genes with greater up-regulation in the fracture callus of older rats with delayed healing. *J Orthop Res* 25:488–494.
29. Meyer RA Jr, Meyer MH, Tenholder M, et al. 2003. Gene expression in older rats with delayed union of femoral fractures. *J Bone Joint Surg [Am]* 85-A:1243–1254.
30. Colnot C, Thompson Z, Miclau T, et al. 2003. Altered fracture repair in the absence of MMP9. *Development* 130:4123–4133.
31. Lu C, Miclau T, Hu D, et al. 2007. Ischemia leads to delayed union during fracture healing: a mouse model. *J Orthop Res* 25:51–61.
32. Ashraf N, Meyer MH, Frick S, et al. 2007. Evidence for overgrowth after midfemoral fracture via increased RNA for mitosis. *Clin Orthop Relat Res* 454:214–222.
33. Desai BJ, Meyer MH, Porter S, et al. 2003. The effect of age on gene expression in adult and juvenile rats following femoral fracture. *J Orthop Trauma* 17:689–698.
34. Gerstenfeld LC, Alkhiary YM, Krall EA, et al. 2006. Three-dimensional reconstruction of fracture callus morphogenesis. *J Histochem Cytochem* 54:1215–1228.
35. Bergmann G, Graichen F, Rohlmann A. 1993. Hip joint loading during walking and running, measured in two patients. *J Biomech* 26:969–990.
36. Bergmann G, Deuretzbacher G, Heller M, et al. 2001. Hip contact forces and gait patterns from routine activities. *J Biomech* 34:859–871.
37. Duda GN, Eckert-Hubner K, Sokiranski R, et al. 1998. Analysis of inter-fragmentary movement as a function of musculoskeletal loading conditions in sheep. *J Biomech* 31:201–210.
38. Taylor WR, Ehrig RM, Heller MO, et al. 2006. Tibio-femoral joint contact forces in sheep. *J Biomech* 39:791–798.
39. Clarke KA, Smart L, Still J. 2001. Ground reaction force and spatiotemporal measurements of the gait of the mouse. *Behav Res Methods Instrum Comput* 33:422–426.
40. Howard CS, Blakeney DC, Medige J, et al. 2000. Functional assessment in the rat by ground reaction forces. *J Biomech* 33:751–757.
41. Gushue DL, Houck J, Lerner AL. 2005. Rabbit knee joint biomechanics: motion analysis and modeling of forces during hopping. *J Orthop Res* 23:735–742.
42. Miyamoto T, Suda T. 2003. Differentiation and function of osteoclasts. *Keio J Med* 52:1–7.
43. Buckwalter JA, Glimcher MJ, Cooper RR, et al. 1996. Bone biology. I: structure, blood supply, cells, matrix, and mineralization. *Instr Course Lect* 45:371–386.
44. Buckwalter JA, Glimcher MJ, Cooper RR, et al. 1996. Bone biology. II: formation, form, modeling, remodeling, and regulation of cell function. *Instr Course Lect* 45:387–399.
45. Hernandez CJ, Majeska RJ, Schaffler MB. 2004. Osteocyte density in woven bone. *Bone* 35:1095–1099.
46. Mullender MG, Huiskes R. 1995. Proposal for the regulatory mechanism of Wolff's law. *J Orthop Res* 13:503–512.
47. Isaksson H, Wilson W, Van Donkelaar CC, et al. 2006. Comparison of biophysical stimuli for mechano-regulation of tissue differentiation during fracture healing. *J Biomech* 39:1507–1516.
48. Lacroix D, Prendergast PJ. 2002. A mechano-regulation model for tissue differentiation during fracture healing: analysis of gap size and loading. *J Biomech* 35:1163–1171.
49. Ruimerman R, van Rietbergen B, Hilbers P, et al. 2005. The effects of trabecular-bone loading variables on the surface

- signaling potential for bone remodeling and adaptation. *Ann Biomed Eng* 33:71–78.
50. Mullender MG, Huiskes R, Versleyen H, et al. 1996. Osteocyte density and histomorphometric parameters in cancellous bone of the proximal femur in five mammalian species. *J Orthop Res* 14:972–979.
51. Mullender MG, Huiskes R. 1995. Proposal for the regulatory mechanism of Wolff's law. *J Orthop Res* 13:503–512.
52. Eriksen EF, Kassem M. 1992. The cellular basis of bone remodeling; the changing architecture of the skeleton. *Sandoz J Med Sci* 31:45–57.